NANOSTRUCTURE AND MAGNETOSTRICTION IN NOVEL DISCONTINUOUS *Terfecohan*/YFe EXCHANGE-SPRING TYPE MULTILAYERS

Do Thi Huong Giang, Nguyen Huu Duc[1], Pham Thi Thuong

Cryogenic Laboratory, Department of Physics, College of Sciences - VNU

Abstract. Sputtered $Tb(Fe_{0.55}Co_{0.45})_{1.5}/Y_xFe_{1-x}$ multilayers ($0 \le x \le 0.2$) with a TbFeCo layer thickness t_{TbFeCo} = 12 nm and YFeCo layer thickness t_{YFeCo} = 10 nm have been studied by means of the X-ray diffraction (XRD), high-resolution transmission electron microscopy (HR-TEM), conversion electron Mössbauer spectrometry (CEMS) and magnetostriction investigations. The results show that nanocrystals are naturally formed and coexist within an amorphous matrix in $Y_{0.1}Fe_{0.9}$ layers. For this discontinuous exchange-spring multilayers, a parallel magnetostrictive susceptibility $\chi_{\lambda//}$ as large as 29.4×10^{-2} T^{-1}, which is almost half of that (79.6×10^{-2} T^{-1}) of the Metglas 2605SC, was achieved.

1. Introduction

Magnetostrictive materials are transducer materials (as well as piezoelectric and shape memory ones), which directly convert electrical energy into mechanical energy. They are useful in the manufacture of microactuators as well as microsensors [1-3]. The performance of microactuators is primarily determined by the value of the magnetostriction (λ), which is the dimensional change resulting from the orientation of magnetization from one direction to another. The performance of microsensors, however, depends rather on the value of the (parallel) magnetostrictive susceptibility, $\chi_{\lambda//} = d\lambda_{//}/dB$, which represents the magnetostrictive response to an applied field. For these applications, transducer materials in the form of thin films are of special interest because cost-effective mass production is possible, compatible to microsystem process technologies.

Most papers concerning giant magnetostriction published in the last decade have been devoted to rare-earth based films and multilayers. As a tradition, various attempts have been mainly focused on amorphous *Terfenol* (a-$TbFe_2$) and *Terfenol-D* (a-$TbDyFe_2$) alloys (*Ter* for Tb, *D* for Dy, *fe* for Fe and *nol* for Naval Ordnance Laboratory, where these alloys were discovered) [4]. In the amorphous state, however, it is strongly preferable to substitute the iron by cobalt, because the amorphous alloys are near the composition a-$TbCo_2$, that presents higher ordering temperatures and higher magnetostriction than the equivalent Fe-based alloy [5].

[1] *Permanent address: Academic Affairs Department, VNU, 144 Xuan Thuy Road, Cau Giay, Hanoi E-mail: ducnh@vnu.edu.vn*

Because of the important role of the "Laboratoire Louis Néel" (Grenoble, France) in their development, we have proposed to refer to the *a*-$TbCo_2$, as "*a-Terconéel*," by an obvious analogy to *Terfenol*. In fact, the magnetostriction has been optimized in a series of thin films of the type a-(Tb,Dy)$(Fe,Co)_2$ (a-*Terfeconéel-D*) [6,7]. In Hanoi, we have developed the amorphous $Tb(Fe_{0.55}Co_{0.45})_{1.5}$ film (named *a-Terfecohan*, here *han* means Hanoi, *i.e.* the capital where studies of this composition have been carried out [6,7]). Still better performances were obtained on magnetostrictive spring-magnet multilayers, where the saturation field of the magnetostrictive *a*-TbDyFeCo phase is lowered by increasing the average magnetisation through exchange coupling with the soft-magnetic FeCo layers [2,3 and refs. therein].

The conventional multilayered concept is usually associating magnetic hard with soft layers, which are structurally homogeneous in either crystalline or amorphous state – named as continuous exchange-spring configuration. In this case, magnetization reversal is thought to be nucleated within the soft layer at low applied field and propagates from the soft layers into the magnetostrictive layers [8,9]. The nucleation of reversal usually occurs at defect points on the sample surface and at interfaces. In this context, one expects that the reversal can be easier nucleated in discontinuous soft phase, *i.e.* in layers in which the FeCo nanograins are embedded within a non-magnetic matrix. The idea to prepare this novel discontinuous exchange-spring type multilayer was applied for {Terfecohan/YFeCo} multilayers by using the bottom-up approach [6]. In this paper, we report a direct approach to obtain the naturally formed nanostructure by controlling the Y-concentration in $\{Terfecohan/Y_xFe_{1-x}\}$ multilayers, that shows a great potential to optimize both large magnetostriction and large magnetostrictive susceptibility.

2. Experimental

$\{TerfecoHan/Y_xFe_{1-x}\}_n$ multilayers with $x = 0, 0.1, 0.2$, $n = 50$ and the individual layer thicknesses $t_{TbFeCo} = 12$ nm and $t_{FeCo} = 10$ nm were fabricated by rf-magnetron sputtering at the Center for Materials Science (College of Natural Science, VNU). Composite targets were consisted of segments of different elements (here Tb, Y, Fe, Co) (fig. 1a). The typical plasma image for sputtering power of 200 W and the Ar pressure of 10^{-2} mbar is showed in fig. 1b. The substrates were glass microscope cover-slips with a nominal thickness of 150 μm. Both target and sample holders were water-cooled.

The crystal structure of samples were studied by X-ray diffraction using the D5005 Siemens with a cooper anticathode. The sample nanostructure was investigated using high-resolution transmission electron microscopy (HRTEM) at the Institute of Physics, Chemnitz University of Technology (Germany). The conversion electron Mössbauer spectrometry (CEMS) was recorded using a

conventonal spectrometer equipped with a homemade helium-methane proportonal counter. The source was a ^{57}Co in rhodium matrix.

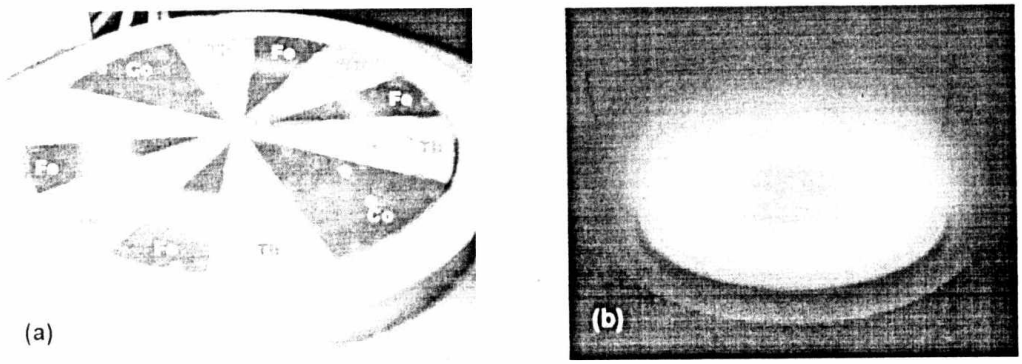

Fig. 1. Composite Terfecohan taget (a) and its plasma in RF sputtering (b)

The magnetostriction was measured using an optical deflectometer (resolution of 5×10^{-6} rad), in which the bending of the substrate due to the magnetostriction in the films was determined.

3. Experimental results and discussions

3.1. Nanostructure

The X-ray 0–2θ diffraction results of the investigated *Terfecohan*/Y_xFe_{1-x} multilayers are shown in fig. 2. One observes a narrow and large intensity diffraction pick at 2θ = 45° in the x = 0 sample, characteristics of the (110) reflections of bcc-Fe. No other diffraction peaks are observed indicating that the *Terfecohan* layers are amorphous. The intensity of the (110) reflection pick is strongly reduced for x = 0.1. This is attributed to the formation of bcc-Fe nanograins. Finally, the (110) reflection almost disappears at x = 0.2 reflecting the fact that the whole multilayer is now amorphous. The corresponding electron diffraction patterns (fig. 3a-c) reinforce further the conclusions of the X-ray analysis. The amorphous state existing in *Terfecohan* layers is characterized by the (typical) first bright spread ring from the inside diffraction spot, whereas the other rings, which are characteristics of the Y_xFe_{1-x} layers, exhibit drastically different behaviours with the variable Y-concentration. They are almost complete sharp rings for x = 0 (fig. 3a) and spotty rings for x = 0.1 (fig. 3b) indicating the crystalline state of Fe layers and the nanocrystalline state of the $Y_{0.1}Fe_{0.9}$ layers, respectively. For x = 0.2, these rings become spread (fig. 3c) that evidence for the amorphous state of $Y_{0.2}Fe_{0.8}$ layers.

A periodic stripe structure of smooth and unsmooth layers in HRTEM-cross-sectional micrograph viewed in Fig. 4a is a good evidence for the multilayered structure of continuous (amorphous) *Terfecohan* layers and discontinuous (nanocrystalline) $Y_{0.1}Fe_{0.9}$ layers. Dark spots observed in unsmooth stripes are

noticeable with an average size of the stripe thickness. They are attributed to bcc-Fe nanograins with an average diameter of about 10 nm. These nanograins are considered as the origin for the weak X-ray diffraction peak and bright spots in the electron diffraction patterns already mentioned above in fig. 2 and 3b. Similar behavior was observed for {*Terfecohan*/$Y_{0.1}(Fe,Co)_{0.9}$} multilayers [8]. For x = 0.2, however, the amorphous state results in a periodic, smooth and homogenous stripe structure, see fig. 4b.

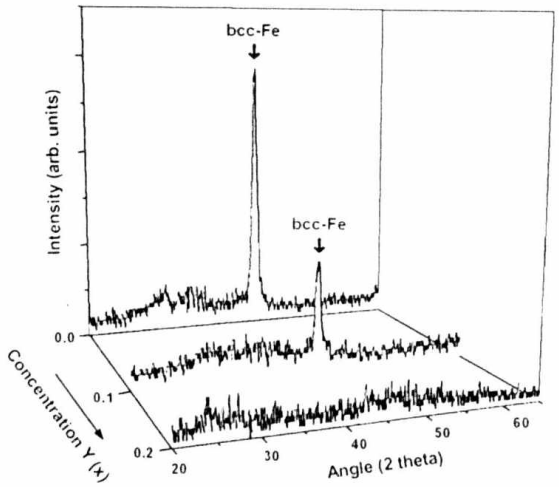

Fig 2. X-ray spectra of as-deposited *Terfecohan*/Y_xFe_{1-x} multilayers

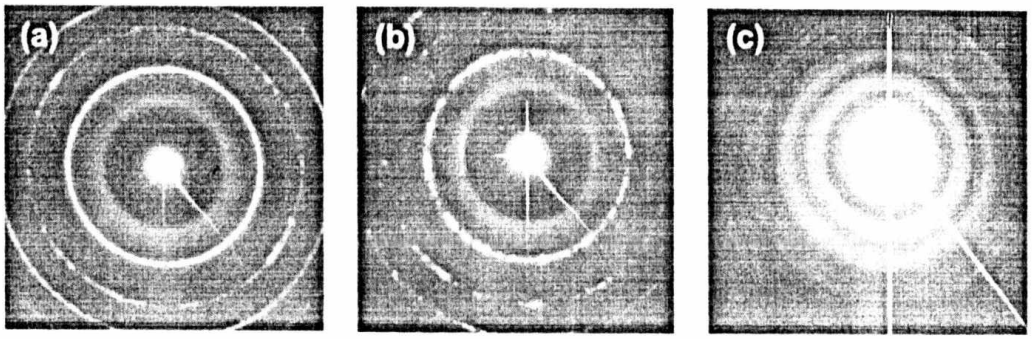

Fig 3. Electron diffraction spectra of as-deposited *Terfecohan*/Y_xFe_{1-x} multilayers

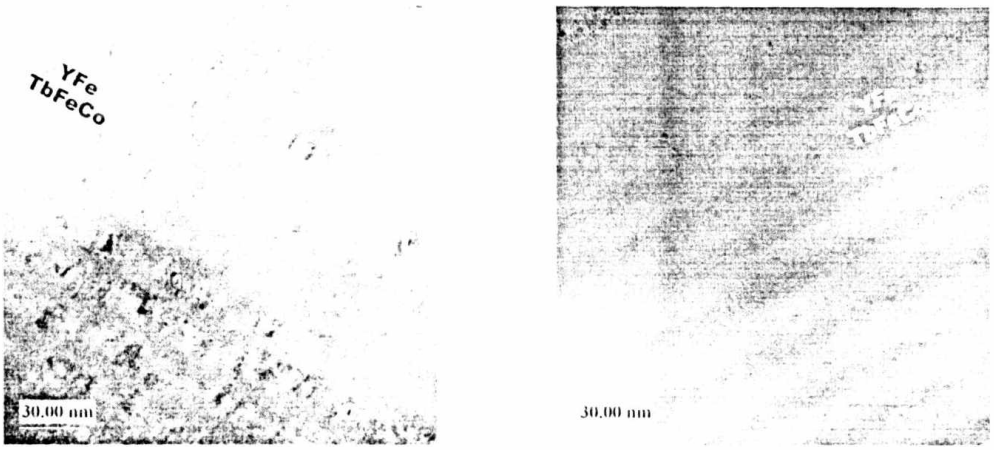

Fig 4. The bright-field high resolution TEM-cross-sectional micrographs of *Terfecohan*/Y_xFe_{1-x} multilayers: (a) x = 0.1 and (b) x = 0.2

The transformation of the amorphous state can be associated to the reduction of the thermodynamic driving force for crystallisation caused by the Y substitution in the Y_xFe_{1-x} layers. Similar behaviour was previously reported for evaporated Z_xFe_{1-x} films [10]. In ref. [10], it was found that the amorphous Fe phase is only stable at small thickness and the crystallisation sets in if the thickness exceeds a critical value of about 2 nm. The critical thickness can, however, reach a value of 30 nm in the $Fe_{93}Zr_7$ film evaporated on Zr base layers. In general, it is possible to note that the transformation of the amorphous state of Fe is shown to be depended on the rare-earth (R and/or Y) concentration. The nanostructure can be naturally formed in as-deposited (R,Y)Fe layers at a critical (R,Y)-concentration (x_c) only. Here $x_c \sim 0.1$. Further increasing rare-earth content stabilizes the amorphous state. This is the reason that the *Terfecohan* phase with high Tb-concentration ($x_{Tb} = 0.4$) always exists in the amorphous state in all investigated samples.

3.2. Mössbauer spectra

Fig. 5 presents the CEM spectra for the as-deposited *Terfecohan*/Y_xFe_{1-x} multilayers. For $x = 0$, the magnetic sextet of bcc-Fe is prominent in the Mössbauer spectra (fig. 5a). The lines of the sextet are broadening and a paramagnetic contribution occurs in the $x = 0.1$ sample (fig. 5b) and finally, the paramagnetic contribution becomes prominent for $x = 0.2$ (fig. 5c). The spectra have been fitted with a wide contribution of hyperfine field to taken into account all the environments experienced by Fe^{57} nuclei. The obtained hyperfine field distributions $P(B_{hf})$ are included in figure 5. For $x = 0$, the $P(B_{hf})$ can be distinguished with two almost separated components: (i) the low hyperfine-field component with an average value of $\langle B_{hf} \rangle = 22$ T and (ii) the high hyperfine-field with $\langle B_{hf} \rangle = 32.5$ T. Taking in to account the fact that the $P(B_{hf})$ of the bcc-Fe is characterised by a peak at $B_{hf} = 32.4$ T, the observed low hyperfine-field ferromagnetic phase can be attributed to the a-*Terfecohan* phase. Indeed, a value of $\langle B_{hf} \rangle = 22$ T was reported for single *Terfecohan* layer film [11]. In addition, it is also able to estimate the Fe fractions, which are of 30 % and 70 % in the *Terfecohan* and Fe layers, respectively. This is in good agreement with those of 28.6 % and 71.4 % deduced for the Fe concentration in the two corresponding layers. For $x = 0.1$ (fig. 5b), the low hyperfine-field ferromagnetic component with $\langle B_{hf} \rangle = 22.5$ T almost remains with fraction $A_{ferr} = 30.5$ %. The fraction of the high hyperfine-field ferromagnetic component (with $\langle B_{hf} \rangle = 31.5$ T) , however, is reduced ($A_{ferr} = 54$ %) and an additional paramagnetic component with $\langle B_{hf} \rangle = 4$ T and $A_{par} = 5.5$ %, has occurred. The measure of the B_{hf} is in agreement with the formation of the Fe nanograins. The high hyperfine-field ferromagnetic fraction almost disappears in the $x = 0.2$ sample (see fig. 5c). For this sample, the major ferromagnetic contribution distributes in a broad hyperfine-field range with a maximum at $B_{hf} = 22$ T and a

fraction A_{ferr} = 65 %. $P(B_{hf})$ shows a minor paramagnetic component with $<B_{hf}> < 10$ T and a fraction A_{par} = 35 %.

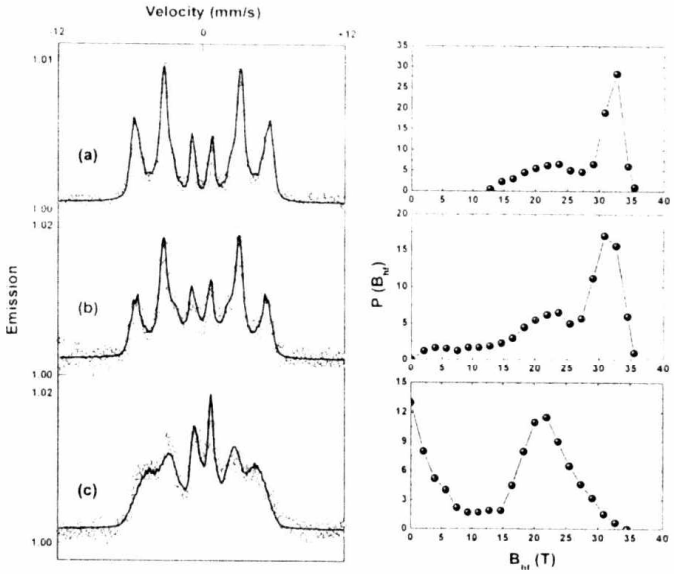

Fig 5. CEMS and hyperfine-field distribution of as-deposited *Terfecohan*/Y_xFe_{1-x} multilayers

3.3. Magnetostriction

The magnetostriction was measured in magnetic fields up-to 0.4 T applied in-plane, parallel and perpendicular to the long side of the sample giving $\lambda_{//}$ and $\lambda_{\perp}$, respectively. The results of λ (= $\lambda_{//}$ - $\lambda_{\perp}$) are presented in fig. 6a for as-deposited films. It is clearly seen that, for x = 0 and 0.1, the magnetostriction is well developed with a rather large magnetostrictive susceptibility at low fields, reaches a maximum and finally decreases at high fields. The observed negative contribution to magnetostriction is related to the formation of an extended domain wall at interfaces, which was already discussed elsewhere [12]. The magnetostriction of x = 0.2 sample is, however, rather difficult to saturate due to its perpendicular anisotropy nature. Low-field parallel magnetostrictive susceptibility data are presented in fig. 6b. The magnetostriction as well as low-field parallel magnetostrictive susceptibility reach maximum values in x = 0.1 sample: λ = 420×10^{-6} and $\chi_{\lambda//}$ = 17.3×10^{-2} T^{-1}. The magnetostriction obtained is comparable to the value deduced from the data of the single-layer samples, *e.g.* λ = 1080×10^{-6} in *Terfecohan* [6,7]. For the x = 0.1 sample, the value of $\chi_{\lambda//}$ is 4 times larger than that of x = 0 and 2 orders larger than that of x = 0.2. This results directly from the low coercivity mechanism proposed above. The (compressive) stresses existing in as-sputtered films are released by low temperature annealing (at $T_A \leq 350$°C for 1 hour). This leads to the change in the orientation of the magnetic easy axis and thus enhances noticeably the saturation magnetostriction and low-field parallel magnetostrictive susceptibility. This is clearly evidenced in fig. 7. For x = 0.1 sample, a large saturation magnetostriction λ = 720×10^{-6} but a low coercivity of 1.1 mT can be

reached. Consequently, $\chi_{\lambda//}$ achieves a maximal value as large as 29.7×10^{-2} T^{-1} at $\mu_0 H$ = 2.1 mT. The obtained $\chi_{\lambda//}$ value is almost 30 times higher than that obtained in *Terfenol-D* and 4 times higher than that obtained in multilayers by Quandt *et. al.* [13,14]. In comparison with the magnetostrictive *Metglas* 2605SC ($\chi_{\lambda//} = 79.6 \times 10^{-2}$ T^{-1}), the obtained $\chi_{\lambda//}$ value is still lower [15], but the present sample shows much larger magnetostriction. This spectacular result illustrates the significance of the approach, which we have developed in view of optimizing both magnetostriction and magnetostrictive susceptibility.

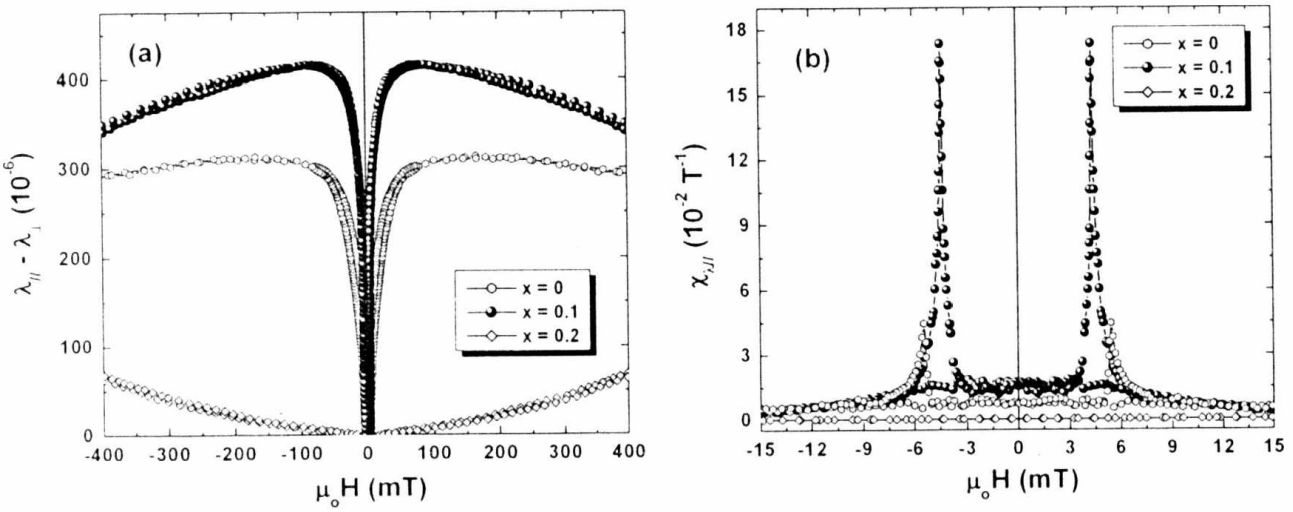

Fig 6. Magnetostriction (a) and parallel magnetostrictive susceptibility hysteresis loops (b) of as-deposited *Terfecohan*/Y_xFe_{1-x} multilayers

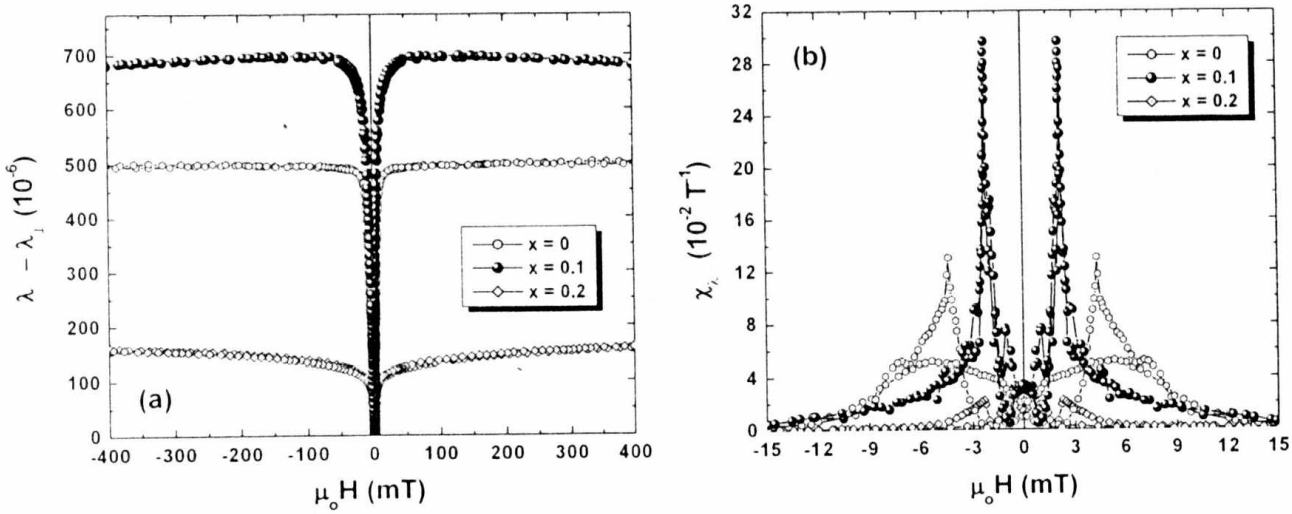

Fig 7. Magnetostriction (a) and parallel magnetostrictive susceptibility hysteresis loops (b) of 350°C-annealed *Terfecohan*/Y_xFe_{1-x} multilayers

4. Concluding remarks

In conclusion, we have described the direct approach to discontinuous magnetostrictive exchange-spring multilayers, in which the nanostructure is naturally formed in YFe soft layers by controlling the Y-concentration. This novel

exchange-spring configuration opens an alternative route towards new high-performance magnetostrictive materials that both large magnetostriction and large magnetostrictive susceptibility can be combined. Furthermore, it provides a new generation of exchange-spring magnetic configuration for studying fundamental reversal mechanism.

Acknowledgement. This work was supported by the State Program for Nanoscience and Nanotechnology of Vietnam under the Project 811.204.

References

1. F. Claeyssen, N. Lhermet , R. Le Letty and P. Bouchilloux, *J. Alloys Compd.* **258**(1997) 61.
2. N.H. Duc, in: *Handbook on Physics and Chemistry of the Rare Earths*, K.A., Gschneirdner, Jr., L. Eyring and G.H. Lande (Elsevier Science, Amsterdam), Vol. **32**(2001) 1.
3. N.H. Duc, P.E. Brommer, in: *Handbook on Magnetic Materials*, K.H.J. Buschow ed., (Elsevier Science, Amsterdam), Vol. **14**(2002) 89
4. A.E. Clark, in: *Ferromagnetic Materials*, ed. E.P. Wohlfarth, (North-Holland, Amsterdam), Vol. **1**(1980) 531.
5. P.E. Brommer, N.H. Duc, in: *Handbook on Magnetic Materials*, K.H.J. Buschow ed., (Elsevier Science, Amsterdam), Vol. **12**(1999) 259.
6. N.H. Duc, P.E. Brommer, in: *Encyclopedia of Materials: Science and Technology*, K.H.J. Buschow ed., (Elsevier Science, Amsterdam), (2004).
7. N.H. Duc, *J. Magn. Magn. Mater.*, **242-245**(2002) 1411.
8. N.H. Duc, D.T. Huong Giang, N. Chau, *J. Magn. Magn. Mater.*, **265**(2004).
9. D.T. Huong Giang, N.H. Duc, V.N. Thuc, L.V. Vu, N. Chau, *J. Appl. Phys. Lett.*, (2004), in press.
10. U. Herr, H. Geisler, H. Ippach and K. Samwer, *Phys. Rev.*, B **59**(1999) 13719.
11. T.M. Danh, N.H. Duc, H.N. Thanh and J. Teillet, *J. Appl. Phys.*, **87**(2000) 7208.
12. N. H. Duc, D. T. Huong Giang, V. N. Thuc, I. Davoli, F. Richomme, *J. Magn. Magn. Mater.*, (2004), *in press*.
13. E. Quandt, A. Ludwig, J. Betz, K. Mackay, D. Givord, *J. App. Phys.* **81**(1997) 5420.
14. Ludwig, E. Quandt, *J. Appl. Phys.* **87**(2000) 4691.
15. E. Trémolet de Lacheisserise, D. Gignoux, M. Schlenker, *Materials and Applications, Magnetism*, Kluwer Academic Publisher, Vol. **2**(2002) 227.